Eur. J. Biochem. *141*, 119–129 (1984)

A nuclear-Overhauser-enhancement study of the solution structure of a double-stranded DNA undecamer comprising a portion of the specific target site for the cyclic-AMP-receptor protein in the *gal* operon

Sequential resonance assignment

G. Marius CLORE and Angela M. GRONENBORN

Division of Physical Biochemistry, National Institute for Medical Research, Mill Hill, London

(Received December 1, 1983/February 1, 1984) – EJB 83 1288

A 500-MHz ^{1}H-NMR study on a double-stranded non-self-complementary DNA undecamer comprising a portion of the specific target site for the cyclic AMP receptor protein in the *gal* operon is presented. Using pre-steady-state nuclear Overhauser effect (NOE) measurements, all exchangeable imino, non-exchangeable base, methyl, and H1′, H2′ and H2″ sugar proton resonances are assigned in a sequential manner. In addition, some of the H3′ sugar proton resonances are also assigned and some of the exchangeable amino proton resonances identified. The relative magnitudes of the intranucleotide and internucleotide NOEs are indicative of a right-handed B-type conformation for the duplex undecamer in solution.

The cAMP receptor protein (CRP) regulates the transcription of at least 20 genes in *Escherichia coli*, including all catabolite-repressible operons, by binding to specific DNA sites in the presence of cAMP [1–4]. In some cases this interaction stimulates transcription, as in the case of the *lac* [5] and *ara* [6] operons; in other cases it inhibits transcription as in the case of the CRP structural gene [7] and the *ompA* gene [8]. In the case of the *gal* operon binding of the cAMP · CRP complex to a single site exerts opposing effects on the P_1 and P_2 promotors, stimulating transcription from the former and inhibiting transcription from the latter [9]. The mechanisms whereby the cAMP · CRP complex exerts these effects are unknown although numerous hypotheses have been put forward [10–14].

From the structural view point, circular dichroic studies have shown that the binding of the cAMP · CRP complex to short oligonucleotides comprising portions of the specific target sites in the *gal* and *lac* operons induces a B to C transition in the structure of the DNA, leaving the handedness of the helix, namely right-handed, unchanged [15, 16]. These findings on small oligonucleotides are completely consistent with the observation that the supercoil unwinding of plasmid DNA achieved by the specific DNA binding of the cAMP · CRP complex is less than 0.5 turn [17]. These results are also consistent with those of DNA melting studies on a 301-base-pair fragment containing the *lac* control region which demonstrated that the binding of the cAMP · CRP complex specifically stabilizes a region of about 36-base-pairs [18].

A deeper understanding of the structural aspects of CRP · DNA interactions can potentially be achieved by two complementary techniques, namely X-ray crystallography and NMR spectroscopy. To date, the crystal structure of the cAMP · CRP complex has been solved at 0.29-nm resolution [12, 19] and NMR studies on CRP and its N-terminal core αCRP, as well as on their interaction with cyclic nucleotides, have been carried out [20–22]. In the present paper we extend the solution NMR studies to the synthetic DNA undecamer (11mer):

5′d(A-A-G-T-G-T-G-A-C-A-T)3′ A stand
3′d(T-T-C-A-C-A-C-T-G-T-A)5′ B stand

which comprises a portion of the specific target site in the *gal* operon [23] and contains eight-base-pairs out of the ten-base-pair consensus, 5′d(A-A-N-T-G-T-G-A-N-N-T-N-N-N-N-C-A) making up specific CRP sites [4]. The interaction of this 11mer with CRP has previously been studied by circular dichroic spectroscopy [15]. Using the nuclear Overhauser effect (NOE) to demonstrate the proximity of protons in space [24–37], all exchangeable imino, non-exchangeable base, methyl, and H1′, H2′ and H2″ deoxyribose proton resonance are assigned in a sequential manner. In addition, some of the H3′ sugar proton resonances are assigned and some of the exchangeable amino proton resonances identified. From the NOE data, qualitative deductions about the solution conformation of the 11mer are made and it is shown that the data are indicative of a right-handed B-type structure.

EXPERIMENTAL PROCEDURE

The two strands of the 11mer, 5′d(A-A-G-T-G-T-G-A-C-A-T) and 5′d(A-T-G-T-C-A-C-A-C-T-T), were prepared from suitably protected nucleosides by the solid-state phosphotriester method and purified by ion-exchange HPLC using a Partisil 10 SAX column essentially as described by Gait et al.

Abbreviations. CRP, cAMP receptor protein of *Escherichia coli* (also known as catabolite activator protein or CAP); NOE, nuclear Overhauser effect; 11mer, undecamer; HPLC, high-pressure liquid chromatography.

[38]. After desalting and extensive lyophilisation, equal amounts of the two 11mers were taken up in either 99.96% D_2O or 90% H_2O/10% D_2O cotaining 300 mM KCl, 15 mM potassium phosphate pH* 6.8 (meter reading uncorrected for the isotope effect on the glass electrode) and 0.18 mM EDTA.

All NMR spectra were recorded on a Bruker AM500 spectrometer operating in Fourier-transform mode with quadrature detection. NOE spectra in D_2O were recorded with a 90° observation pulse (pulse length 9 μs), an acquisition time of 0.5 s (8 K data points and an 8.2 kHz spectral width) and a relaxation delay of 1 s. NOE spectra in H_2O were recorded using a time-shared hard 1-1 observation pulse θ_x-τ-θ_x [39] with the carrier placed 3048 Hz downfield from the water resonance, a delay of 160.5 μs and a total flip angle ($2\theta_x$) of 90°; the acquisition time was 0.366 s (8 K data points and a spectral width of 12195 Hz) and the relaxation delay was 1 s. The reference spectra were recorded using a longer acquisition time: 2 s (32 K data points) and 1.46 s (32 K data points) for the spectra in D_2O and H_2O respectively. The NOEs were observed by directly collecting the difference free induction decay (FID) by interleaving 16 transients after saturation for a given length of time (0.4 s or 0.8 s) of a given resonance, with 16 transients of off-resonance irradiation applied for the same length of time. The power of the selective irradiation pulse used was sufficient to achieve effective instantaneous saturation as regards NOE effects (i.e. the high power limit) whilst at the same time maintaining selectivity [40]. NOE magnitudes were obtained as described previously [34]. In the case of the spectra recorded in H_2O, the FIDs were subjected to data shift manipulation [39, 41, 42] prior to Fourier transformation in order to reduce further the intensity of the water resonance, thereby eliminating baseline distortions. Chemical shifts are expressed relative to 4,4-dimethylsilapentane-1-sulfonate.

RESULTS AND DISCUSSION

Assignment of resonance type

The 500-MHz ^{1}H-NMR spectra of the duplex 11mer in 99.96% D_2O (at 23 °C) showing only the non-exchangeable proton resonances, and in 90% H_2O/10% D_2O (at 10 °C and 23 °C) showing both the exchangeable and non-exchangeable proton resonances are illustrated in Fig. 1 and 2 respectively. Under the conditions of ionic strength (300 mM KCl) and temperature employed, the two strands of the 11mer are entirely in the duplex state as judged from thermal denaturation studies (data not shown).

The assignment of resonance type is easily achieved by comparison with the spectra of nucleotides and other small oligonucleotides [34, 36, 37, 43–45]. On this basis, peaks 1–7 are assigned to the methyl protons of the T residues, peaks 8–22 to the H2′ and H2″ sugar protons, peaks 23–41 to the H1′ sugar protons and the H5 protons of the C residues, peaks 42–69 to the H8, H6 and H2 base protons, peaks a–i to the exchangeable imino protons, and peaks j–r to the exchangeable amino protons. Within each region, further distinctions can be made. In the H2′/H2″ region (peaks 8–22), it is generally the case that the H2′ and H2″ resonances of the pyrimidine residues lie to high field of those of the purine residues. In the H1′/H5 region (peaks 23–41), the H5 proton resonances are easily distinguished from the H1′ resonances on account of their multiplet structure: namely, the H5 resonances are doublets due to coupling between the H5 and H6 protons of the C residues whereas the H1′ resonances are triplets due to coupling between the H1′ proton and the H2′ and H2″ protons. Thus peaks 23, 24 and 28 are assigned to H5 protons and peaks 25–27 and 29–41 to H1′ protons. Inversely gated decoupling experiments then enable one to correlate the H5 proton resonance of a given C residue with the H6 proton of the same residue. In this manner, the doublet peaks 44, 45, 47 and 50 are assigned to C(H6) resonances associated with the C(H5) resonances 23, 24, 23 and 28 respectively. (Note that peak 23 contains two superimposed H5 resonances.) The A(H2) resonances are distinguished from the H8 and T(H6) resonances on account of their long spin-spin relaxation times (i.e. narrow linewidths) arising from inefficient relaxation due to the fact that their nearest neighbouring non-exchangeable proton is $\gtrsim$ 0.45 nm away. This can be assessed using the simple 90°-τ-180°-τ spin echo sequence: with a value of τ of 0.25 s, the only resonances detectable in the H8/H6/H2 proton resonance region are peaks 52, 53, 55–58 and 63 which are therefore assigned to the A(H2) protons. The H6 protons of the T residues always lie to high field of the H8 resonances of the A and G residues. On this basis peaks 42, 43, 45, 46, 48, 49 and 51 are assigned to T(H6) protons, and peaks 54, 59–62, 64–68 and 69 to H8 protons of A and G residues. Finally in the imino proton resonance region the hydrogen-bonded imino proton resonances of G · C base pairs lie to high field of those of the A · T base pairs, thereby enabling the assignment of peaks f–i to the former and peaks a–e to the latter.

It will be noted that whereas all four G(H1) imino proton resonances are clearly visible, only five out of the seven T(H3) imino protons are detectable. This is due to kinetic fraying of the terminal A · T base pairs, 1 and 11, so that the corresponding T(H3) imino proton resonances are exchange-broadened beyond detectability. In addition, the T(H3) imino proton resonances a and e are broad even at temperatures below 10 °C and disappear at temperatures above 20 °C and 25 °C respectively; on this basis resonances a and e can be assigned to the penultimate A · T base pairs, 2 and 10.

Sequential resonance assignment

In order to assign each resonance to a particular proton we have made exclusive use of pre-steady-state NOE measurements [40, 46]. For short irradiation times, the magnitude of the NOE, N_{ij}, observed on the resonance of proton i following irradiation of the resonance of proton j, is given by

$$N_{ij} \approx \sigma_{ij} t \qquad (1)$$

where σ_{ij} is the cross-relaxation rate between protons i and j and t is the length of the irradiation time. (Note that N_{ij} and σ_{ij} are negative as, for molecules the size of the double-stranded undecamer, $\omega\tau_c \gg 1$.) The cross-relaxation rate σ_{ij} is proportional to r_{ij}^{-6} where r_{ij} is the distance between the two protons i and j. As a result, the magnitude of the pre-steady-state NOE is very sensitive to inter-proton distance, decreasing rapidly as r_{ij} increases and becoming virtually undetectable for $r_{ij} \gtrsim 0.5$ nm. This feature of the NOE simultaneously provides a method for sequential resonance assignment and a sensitive probe of molecular structure. NOE sequential resonance assignment strategies for oligonucleotides, based on the known structures of right-handed DNA, have been extensively discussed [33–37]. A comprehensive strategy for the assignment of the exchangeable annd non-exchangeable base proton resonances, the methyl proton resonances and the H1′, H2′, H2″ and H3′ sugar resonances in right-handed double-

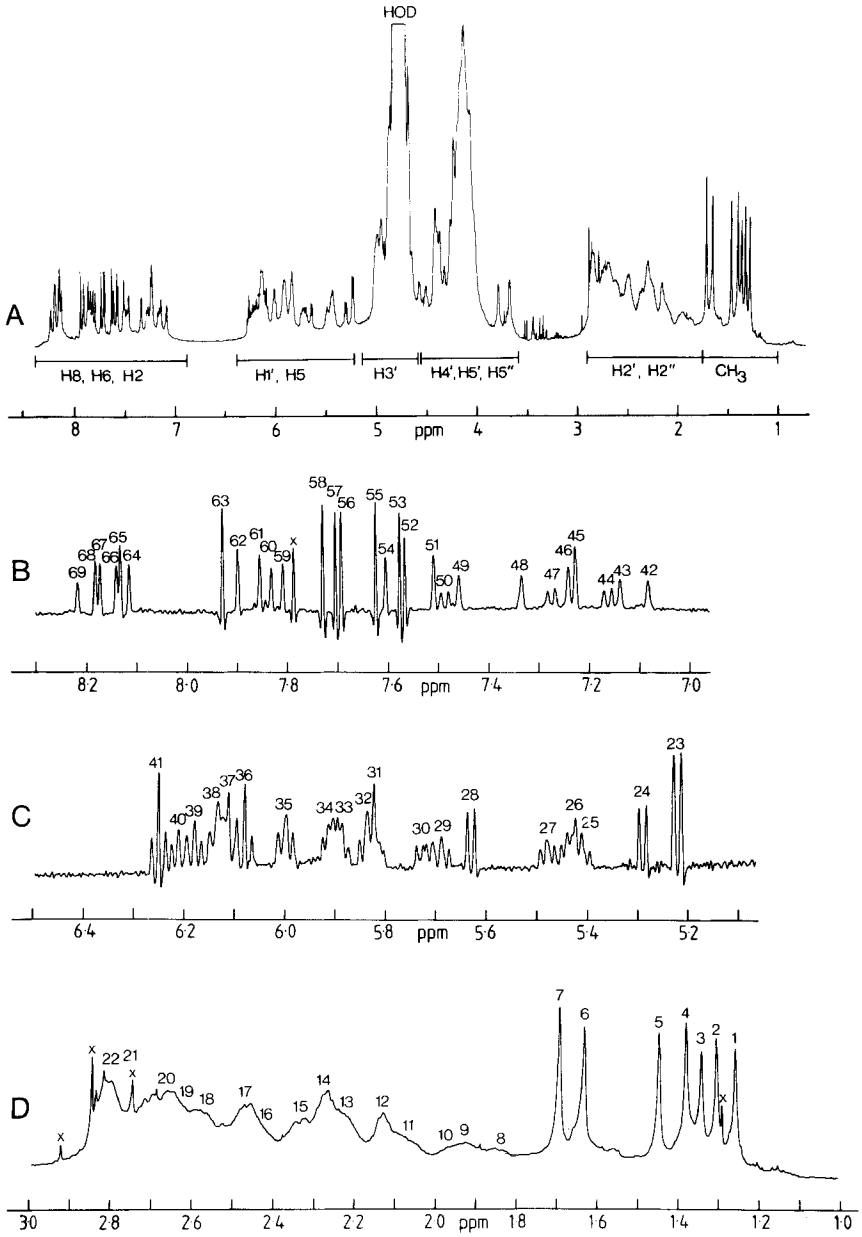

Fig. 1. *500-MHz ^{1}H-NMR spectrum of the duplex 11mer in 99.96% D_2O at 23 °C.* (A) Complete spectrum between 1.0 ppm and 8.5 ppm. (B) Resolution-enhanced expansion of the H8/H6/H2 resonance region between 7.0 ppm and 8.3 ppm. (C) Resolution-enhanced expansion of the H1′/H5 resonance region between 5.1 ppm and 6.5 ppm. (D) Expansion of the CH_3 and H2′/H2″ resonance regions between 1.0 ppm and 3.0 ppm. The assignments of the numbered resonances are given in Table 4. Experimental conditions: 2 mM duplex 11mer in 99.96% D_2O containing 300 mM KCl, 15 mM potassium phosphate pH* 6.8 and 0.18 mM EDTA. The peaks marked x arise from low-molecular-mass impurities. The expansions shown in B and C were resolution-enhanced by multiplying the free induction decay by a two-term exponential function (Lorentz-Gauss multiplication) prior to Fourier transformation

stranded DNA helices is summarized in Fig. 3. Particular attention is drawn to those internucleotide NOEs with directional content.

Assignment of the non-exchangeable proton resonances

Assignment of the non-exchangeable proton resonances of the duplex 11mer was based entirely on systematic pre-steady-state NOE measurements, irradiating all the numbered resonances in Fig. 1 in turn. The NOEs relating to the A strand, the B strand and inter-strand effects are given in Tables 1, 2 and 3 respectively. All observed NOEs were reciprocal with the exception of those between the H1 and A(H2) protons. Here, only NOEs on the A(H2) resonances following irradiation of the H1′ resonances could be observed, and not vice versa. The reason for the absence of reciprocity is simple: namely, NOEs observed between these protons are very small ($\approx -1\%$) and, consequently, are more easily detected on the narrow A(H2) resonances than on the broader H1′ resonances. Using the sequential resonance assignment scheme shown in Fig. 3, the NOE data set in Tables 1 – 3 can be interpreted to yield unambiguous assignments of all the non-exchangeable base, methyl, H1′, H2′ and H2″ resonances. In addition, some of the H3′ resonances could also be assigned by means of in-

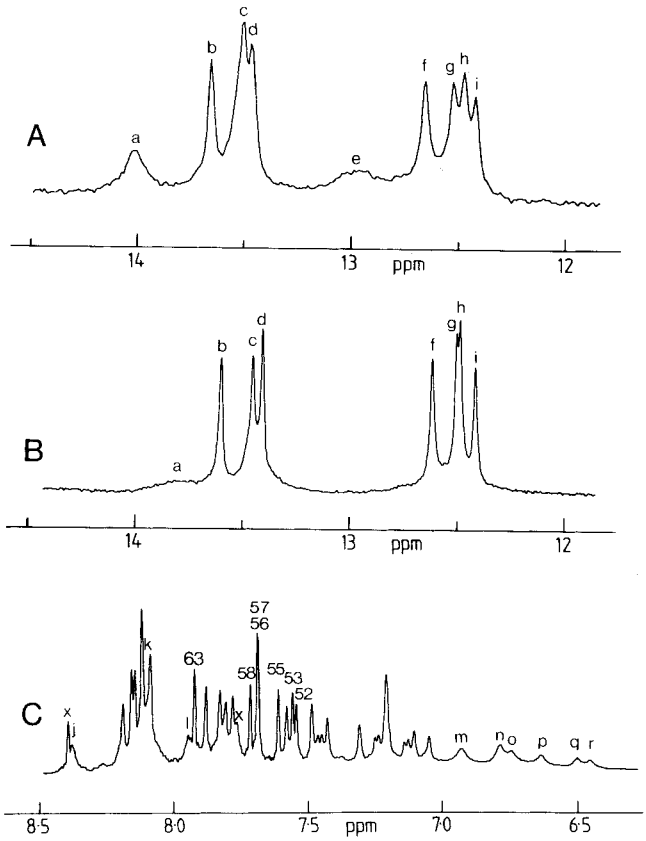

Fig. 2. *500-MHz ^{1}H-NMR spectra of the duplex 11mer in 90% H_2O/10% D_2O.* (A) Imino proton resonance region (12.0 – 14.5 ppm) at 10 °C. (B) Imino proton resonance region (12.0 – 14.5 ppm) at 23 °C. (C) H8/H6/H2/amino proton resonance region (6.5 – 8.5 ppm) at 23 °C. The exchangeable proton resonances are labelled a – r and the A(H2) resonances are numbered as in Fig. 1. The assignments of the exchangeable proton resonances are given in Table 4. The experimental conditions are the same as those in the Fig. 1 legend except that the sample is in 90% H_2O/10% D_2O. The peaks marked x arise from low-molecular-mass impurities

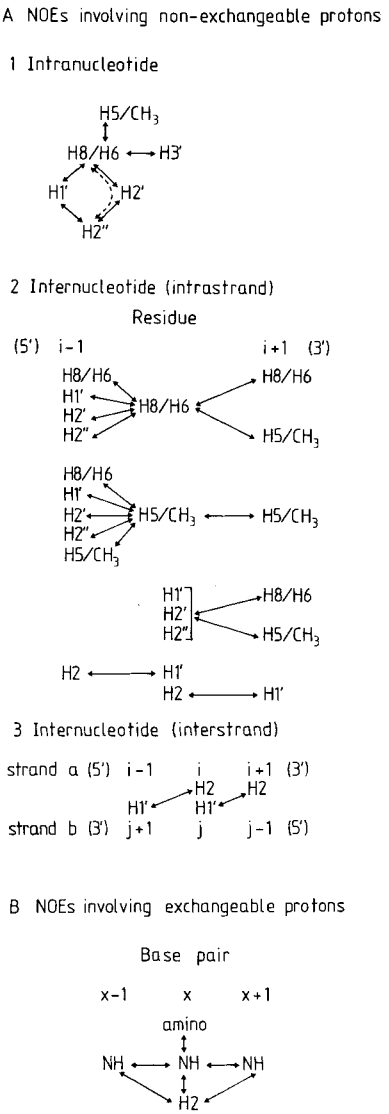

Fig. 3. *Schematic illustration of the intranucleotide and internucleotide interproton distances with values of $\lesssim 0.5$ nm in right-handed DNA which form the basis of the sequential resonance assignment procedure by means of NOE measurements.* The diagram is restricted to interproton distances involving the H8/H6/H2 base protons, the methyl protons, the H1″, H2′, H2″ and H3′ sugar protons and the exchangeable imino and amino protons. These distance relationships are applicable to both B and A DNA [34, 36, 37, 49]. (The interrupted line between the H8/H6 and H2″ protons of the same residue indicates that, although these protons are separated by $\lesssim 0.5$ nm, the major contribution to the intranucleotide NOE between these protons arises not from direct cross-relaxation but from indirect cross-relaxation via the H2′ proton due to the very close proximity, 0.18 nm, of the H2′ and H2″ protons)

tranucleotide NOEs observed in the H3′ resonance region (4.7 – 5.0 ppm) following irradiation of the H8/H6 base proton resonances. All assignments are given in Table 4. It goes without saying that the interpretation of the complete NOE data set was thoroughly checked for self-consistency as this stringent requirement provides an easy and reliable check for possible assignment errors [30 – 37, 47].

Some examples of pre-steady-state NOE difference spectra relating to the terminal residues of both strands are shown in Fig. 4. Except where stated, the irradiation time used was 0.8 s which was sufficient to allow sizeable direct NOEs to build up whilst ensuring that most second-order spin-diffusion effects were kept to a minimum.

Considering the B strand first, we note that the sequence d(C-T-T) of the three terminal residues is unique in the duplex, thereby giving one an easy entry into the sequential assignment of the B strand resonances via the well resolved methyl proton resonances. Irradiation of the T(CH_3) resonance 7 (Fig. 4A) results in NOEs on two T(H6) resonances (peaks 51 and 49), an H1′ resonance (peak 37) and an H2′/H2″ resonance (peak 13). The magnitude of the NOE on peak 51 is $\approx -20\%$ whilst that on peak 49 is $\approx -10\%$. Given that there is only a single occurrence of a d(T-T) sequence and that, in the case of right-handed DNA, irradiation of a T(CH_3) resonance will give rise to a large intranucleotide NOE on a T(H6) resonance, and smaller internucleotide NOEs on the H8/H6, H1′, H2′ and H2″ resonances of the 5′ residue, immediately enables one to assign peaks 7 and 51 to the CH_3 and H6 protons, respectively, of T_{11B}, and peaks 49, 37 and 13 to the H6, H1′ and H2′/H2″ protons, respectively, of T_{10B}. The identification of the H1′, H2′ and H2″ resonance of T_{11B} can be achieved by irradiation of the T_{11B}(H6) resonance 51 (spectrum not shown) which results in intranucleotide NOEs on the T_{11B}(CH_3) (peak 7),

Table 1. *NOEs involving the non-exchangeable proton resonances of the A strand, 5′d(A-A-G-T-G-T-G-A-C-A-T) of the duplex 11mer*
NOEs were observed in 99.96% D_2O at 23 °C using an irradiation time of 0.8 s and the experimental conditions are given in the legend to Fig. 1. The magnitude of the NOEs are represented by the following symbols: l (large), $\gtrsim -15\%$; m (medium), -5% to -15%; s (small), $\lesssim -5\%$; vs (very small), $\sim -1\%$; ml, on the border of medium and large; ms, on the border of medium and small. The assignments of the peaks based on the NOE measurements are given in Table 4

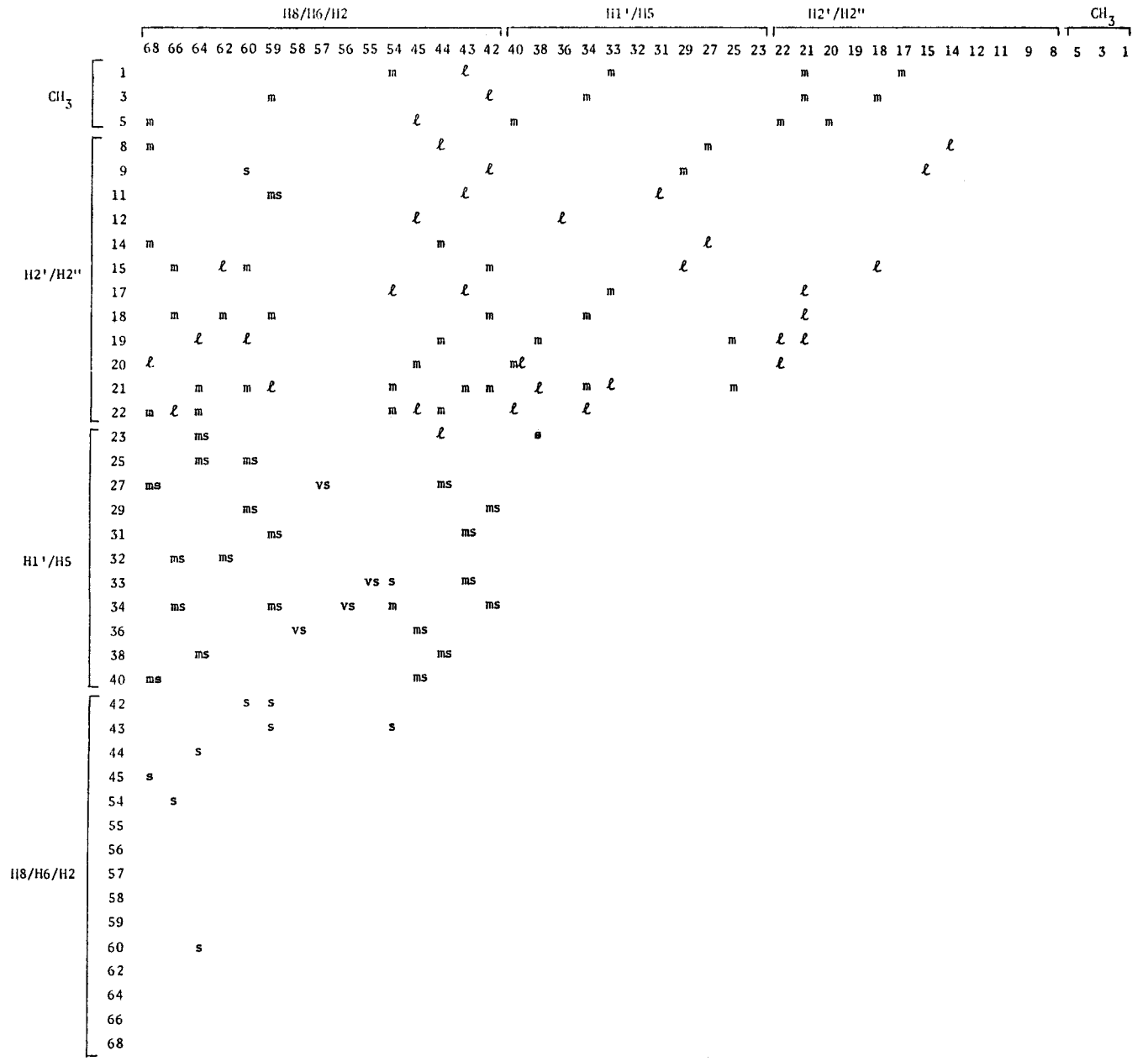

T_{11B}(H1′) (peak 41) and T_{11B}(H2′)/(H2″) (peak 14) resonances, and in the same internucleotide NOEs as observed on irradiation of the $T_{11B}(CH_3)$ resonance. Irradiation of the T_{11B}(H1′) resonance 41 (Fig. 4C) confirms the assignment of the T_{11B}(H6) and T_{11B}(H2′)/(H2″) resonances by giving rise to the expected intranucleotide NOEs on these resonances, and, in addition, results in a very small inter-strand NOE on the A_{2A}(H2) resonance (peak 55). The $T_{10B}(CH_3)$ resonance is easily assigned to peak 6 by the large intranucleotide NOE observed on irradiation of the T_{10B}(H6) resonance 49 (spectrum not shown). Irradiation of the $T_{10B}(CH_3)$ resonance 6 (Fig. 4D) gives rise to the expected large intranucleotide NOE on the T_{10B}(H6) resonance (peak 49), to an indirect intranucleotide NOE via the T_{10B}(H6) proton on the T_{10B}(H2′)/(H2″) resonance (peak 13) and to internucleotide NOEs on the H6 (peak 47), H5 (peak 23), H1′ (peak 31), H2′ (peak 10) and the H2″ (peak 16) resonances of the residue on its 5′ side, C_{9B}. Irradiation of the C_{9B}(H6) resonance peak 47 (Fig. 4E) then results in intranucleotide NOEs on the C_{9B}(H5) (peak 23), C_{9B}(H1′) (peak 31), C_{9B}(H2′) (peak 10) and C_{9B}(H2″) (peak 16) [indirect via C_{9B}(H2′) proton] resonances, an internucleotide NOE on the CH_3 resonance (peak 6) of the

Table 2. *NOEs involving the non-exchangeable proton resonances of the B strand, 5′d(A-T-G-T-C-A-C-A-C-T-T), of the duplex 11mer*
Conditions and symbols are the same as in Table 1

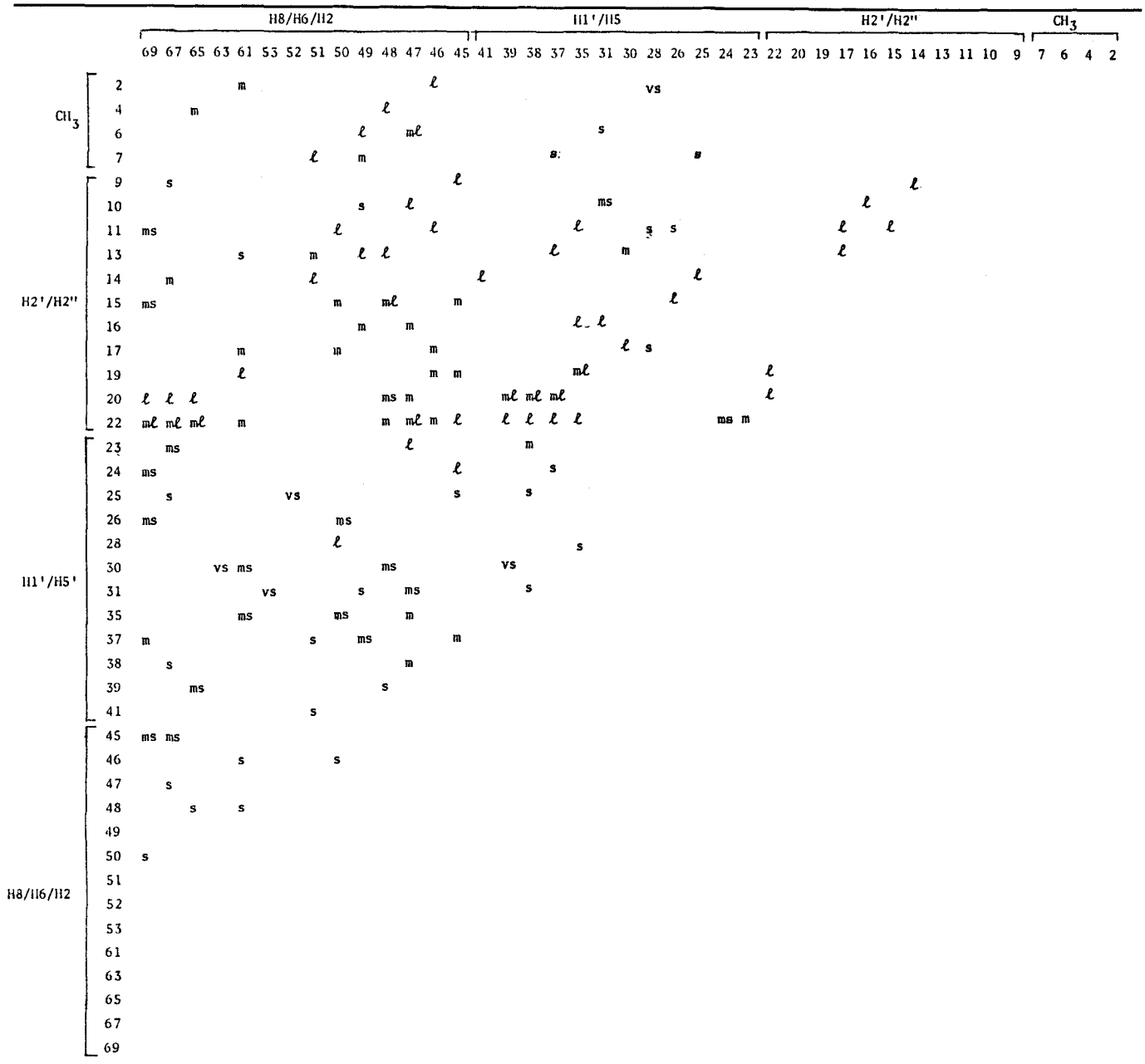

Table 3. *Interstrand NOEs involving the H1′ and H2 resonances of the duplex 11mer*
Conditions and symbols are the same as in Table 1

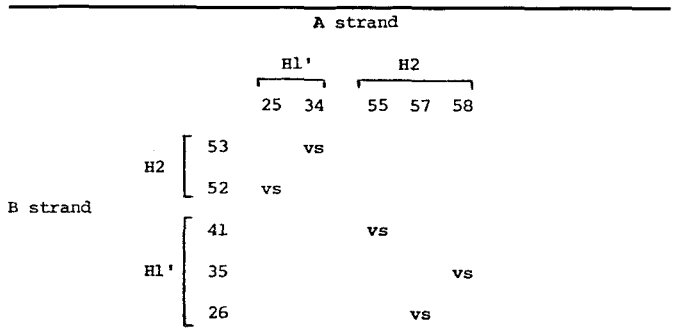

3′ residue T_{10B}, and internucleotide NOEs on the H8 (peak 67), H1′ (peak 38), H2′ (peak 20) and H2″ (peak 22) resonances of the 5′ residue of A_{8B}. The internucleotide NOEs on the H8, H1′ and H2″ resonances of A_{8B} and the CH_3 resonance of T_{10B} are also observed on irradiation of the C_{9B}(H5) resonance 23 (Fig. 4F). [Note that peak 23 also contains the C_{9A}(H5) resonance.]

The same approach can be used to assign sequentially the A strand resonances; as in the case of the B strand, the sequence d(C-A-T) of the three terminal residues is unique in the duplex, thereby simplifying matters. Irradiation of the $T_{11A}(CH_3)$ resonance 5 (Fig. 4G) results in a large intranucleotide NOE on the T_{11A}(H6) resonance (peak 45), an indirect intranucleotide NOE via the T_{11A}(H6) proton on the T_{11A}(H2′)/(H2″) resonance (peak 12), and internucleotide NOEs on the H8

Table 4. *Assignments of the exchangeable and non-exchangeable proton resonances of the duplex 11mer determined by NOE measurements*
Chemical shifts were measured relative to 4,4-dimethylsilopentane-1-sulfonate at 23 °C

Residue	Chemical shift (peak no.) of protons										
	H8	H6	H5	CH_3	H2	H1′	H2′	H2″	H3′	N1H	N3H
A chain	ppm										
A_{1A}	7.90 (62)				7.70 (56)	5.84 (32)	2.34 (15)	2.56 (18)	5.06		
A_{2A}	8.15 (66)				7.63 (55)	5.90 (34)	2.81 (22)	2.81 (22)	–		
G_{3A}	7.61 (54)					5.88 (33)	2.47 (17)	2.71 (21)	5.06	12.61 (f)	
T_{4A}		7.14 (43)		1.25 (1)		5.83 (31)	2.10 (11)	2.10 (11)	–		13.41 (d)
G_{5A}	7.81 (59)					5.90 (34)	2.71 (21)	2.55 (18)	–	12.41 (i)	
T_{6A}		7.08 (42)		1.34 (3)		5.69 (29)	1.91 (9)	2.30 (15)	–		13.45 (c)
G_{7A}	7.83 (60)					5.41 (25)	2.63 (19)	2.71 (21)	–	12.49 (g)	
A_{8A}	8.12 (64)				7.71 (57)	6.14 (38)	2.61 (19)	2.71 (21)	4.98		
C_{9A}		7.16 (44)	5.22 (23)			5.48 (27)	1.85 (8)	2.26 (14)	4.98		
A_{10A}	8.19 (68)				7.73 (58)	6.22 (40)	2.67 (20)	2.82 (22)	–		
T_{11A}		7.23 (45)		1.44 (5)		6.09 (36)	2.13 (12)	2.13 (12)	–		
B chain											
A_{1B}	8.14 (65)				7.93 (63)	6.19 (39)	2.81 (22)	2.65 (20)	5.06		
T_{2B}		7.34 (48)		1.37 (4)		5.72 (30)	2.21 (13)	2.45 (17)	–		–[a] (e)
G_{3B}	7.86 (61)					6.00 (35)	2.60 (19)	2.77 (22)	4.92	12.50 (h)	
T_{4B}		7.24 (46)		1.30 (2)		6.00 (35)	2.09 (11)	2.45 (17)	–		13.6 (b)
C_{5B}		7.49 (50)	5.64 (28)			5.44 (26)	2.05 (11)	2.33 (15)	–		
A_{6B}	8.22 (69)				7.57 (52)	6.12 (37)	2.67 (20)	2.82 (22)	4.99		
C_{7B}		7.23 (45)	5.29 (24)			5.41 (25)	1.93 (9)	2.29 (14)	–		
A_{8B}	8.18 (67)				7.58 (53)	6.14 (38)	2.67 (20)	2.82 (22)	–		
C_{9B}		7.27 (47)	5.22 (23)			5.83 (31)	1.96 (10)	2.43 (16)	–		
T_{10B}		7.46 (49)		1.63 (6)		6.12 (37)	2.24 (13)	2.24 (13)	–		13.8 (a)
T_{11B}		7.51 (51)		1.69 (7)		6.26 (41)	2.27 (14)	2.27 (14)	4.56		

[a] Resonance e is not detectable above 20 °C; its chemical shift at 10 °C is 12.95 ppm.

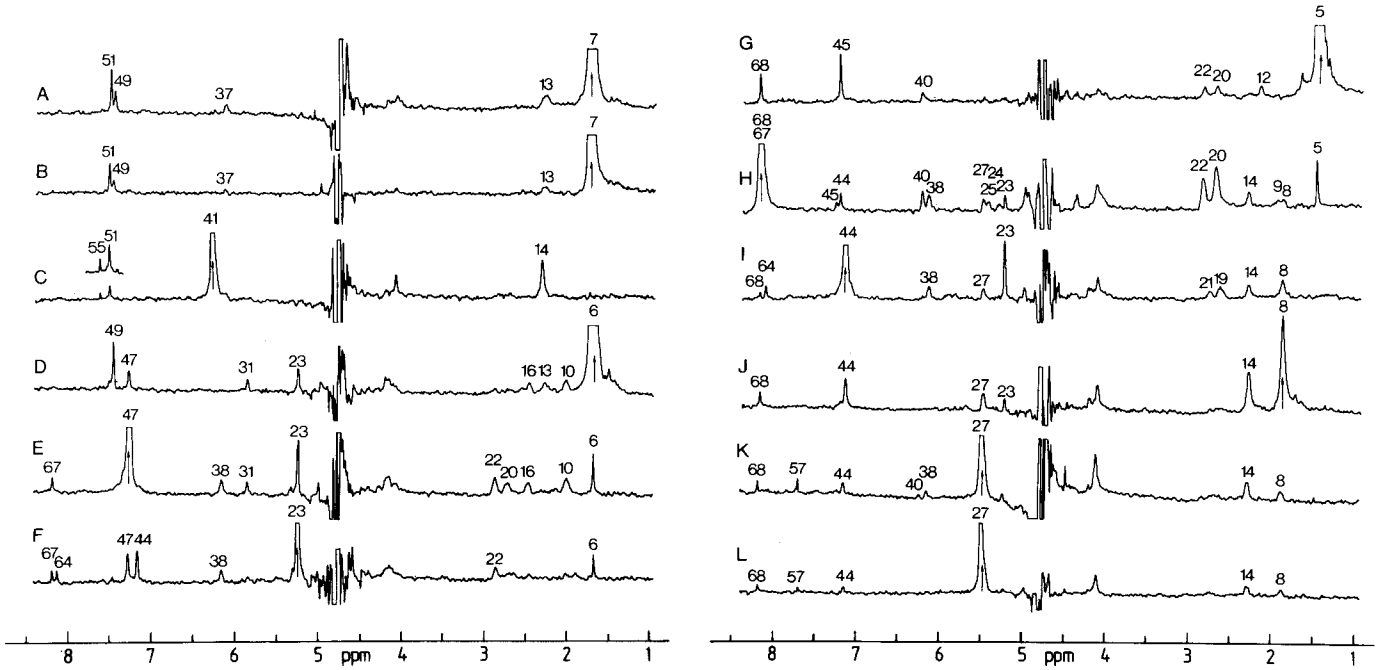

Fig. 4. *500-MHz pre-steady-state NOE difference spectra (off-resonance minus on-resonance irradiation) on the duplex 11mer in 99.96% D_2O at 23 °C following irradiation of various resonance peaks.* (A), (B) The $T_{11B}(CH_3)$ resonance 7; (C) the T_{11B}(H1′) resonance 41; (D) the $T_{10B}(CH_3)$ resonance 6; (E) the C_{9B}(H6) resonance 47; (F) the C_{9B}(H5)/C_{9A}(H5) resonance 23: (G) the $T_{11A}(CH_3)$ resonance 5; (H) the A_{10A}(H8) and A_{9B}(H8) resonances 68 and 67; (I) the C_{9A}(H6) resonance 44; (J) the C_{9A}(H2′) resonance 8; (K, L) the C_{9A}(H1′) resonance 27. The assignments of the other peaks seen in the difference spectra are given in Table 4. Note that a decrease in intensity of a particular resonance is seen as a positive peak in the difference spectrum. The irradiating pulse was applied for 0.8 s for all NOE difference spectra with the exception of B and L where it was applied for 0.4 s. 1600 transients were averaged for each difference spectrum. The experimental conditions are the same as those in Fig. 1

(peak 68), H1′ (peak 40), H2′ (peak 20) and H2″ (peak 22) resonances of the residue on its 5′ side, A_{10A}. Irradiation of the A_{10A}(H8) resonance alone is not feasible as peak 68 closely overlaps with peak 67, the A_{9B}(H8) resonance. Thus, irradiation of peak 67/68 (Fig. 4H) results in a combination of NOEs arising from both the A_{10A}(H8) and A_{8B}(H8) resonances. From the A_{10A}(H8) proton there are intranucleotide NOEs on the A_{10A}(H1′) (peak 40), A_{10A}(H2′) (peak 20) and A_{10A}(H2″) (peak 22) [indirect via A_{10A}(H2′) proton] resonances, an internucleotide NOE on the CH_3 resonance (peak 5) of the 3′ residue T_{11A}, and internucleotide NOEs on the H6 (peak 44), H5 (peak 23), H1′ (peak 27), H2′ (peak 8) and H2″ (peak 14) resonances of the 5′ residue C_{9A}. [The NOEs arising from the A_{8B}(H8) proton are as follows: intranucleotide NOEs on the A_{8B}(H1′) (peak 38), A_{8B}(H2′) (peak 20) and A_{8B}(H2″) (peak 22) resonances, and internucleotide NOEs on the C_{7B}(H6) (peak 45), C_{7B}(H5) (peak 24), C_{7B}(H1′) (peak 25), C_{7B}(H2′) (peak 9) and C_{7B}(H2″) (peak 14) resonances.] Irradiation of the C_{9A}(H6) resonance 44 (Fig. 4I) results in intranucleotide NOEs on the C_{9A}(H5) (peak 23), C_{8A}(H1′) (peak 27), C_{9A}(H2′) (peak 8), C_{9A}(H2″) (peak 14) [indirect via C_{9A}(H2′) proton] and C_{9A}(H3′) (4.98 ppm) resonances, an internucleotide NOE on the H8 resonance (peak 68) of the 3′ residue A_{10A}, and internucleotide NOEs on the H8 (peak 64), H1′ (peak 38), H2′ (peak 19) and H2″ (peak 21) resonances of the 5′ residue A_{8A}. [The internucleotide NOEs on the H8 and H1′ resonances of the A_{8A} residue are also observed on irradiation of the C_{9A}(H5) resonance 23; see Fig. 4F.] Fig. 4J illustrates the NOEs observed on irradiation of the C_{9A}(H2′) resonance 8: there are direct intranucleotide NOEs on the C_{9A}(H2″) (peak 14), C_{9A}(H1′) (peak 27) and C_{9A}(H6) (peak 44) resonances, a small indirect intranucleotide NOE via the C_{9A}(H6) proton on the C_{9A}(H5) resonance (peak 23), and an internucleotide NOE on the H8 resonance (peak 68) of the 3′ residue A_{10A}. These findings are confirmed by irradiation of the C_{9A}(H1′) resonance 27 (Fig. 4K) which results in intranucleotide NOEs on the C_{9A}(H6) (peak 44), C_{9A}(H2′) (peak 8) and C_{9A}(H2″) (peak 14) resonances, internucleotide NOEs on the H8 (peak 68) and H1′ (peak 40) resonances of the 3′ residue A_{10A}, and internucleotide NOEs on the H1′ (peak 38) and the H2 (peak 57) resonances of the 5′ residue A_{8A}.

It will be noted that a distinction is made in the above descriptions between the H2′ and H2″ sugar resonances. This is readily made on the basis of two criteria. First, irradiation of the H8/H6 base proton resonance always results in a larger intranucleotide NOE on the H2′ resonance than on the H2″ resonance for all glycosidic bond torsion angles within the *anti* range characteristic of right-handed A and B DNA (e.g. see Fig. 4E, H and I); moreover, within this conformational range, the principal contribution to the observed intranucleotide NOE between the H8/H6 and H2″ protons arises from indirect cross-relaxation via the H2′ proton due to the very short separation of only 0.18 nm between the H2′ and H2″ protons. Second, the intranucleotide NOE between the H1′ and H2″ protons is usually larger and can never be smaller than that between the H1′ and H2′ protons for all sugar pucker conformations (e.g. see Fig. 4K and L). Despite the extensive overlap and poor resolution with the H2′/H2″ resonance region, unambiguous assignments of the H2′ and H2″ resonances can easily be made by one-dimensional NOE difference spectroscopy as the H8/H6/H2, H1′/H5 and CH_3 resonance regions are well resolved.

The effect of irradiation time on the magnitude of the NOEs is also illustrated in Fig. 4. Fig. 4B and 4L show the NOE difference spectra obtained on irradiation of the $T_{11B}(CH_3)$ and C_{9A}(H1′) resonances respectively for 0.4 s. Comparison with the corresponding NOE difference spectra obtained with a 0.8 s irradiation time (Fig. 4A and 4K respectively) clearly shows the increase in size of the NOEs on increasing irradiation time. The increase in some of the NOE magnitudes is slightly less than twofold as, at an irradiation time of 0.8 s, small deviations from the initial rate approximation Eqn (1) are already apparent. Consequently the data at 0.8 s irradiation time cannot be used to obtain accurate distance ratios and distances involving the non-exchangeable protons. Nevertheless, it is ideal both for assignment purposes and for obtaining a qualitative picture of the solution structure of the duplex 11mer since the selectivity of the NOEs is preserved and the relative magnitudes of the NOEs are only minimally distorted.

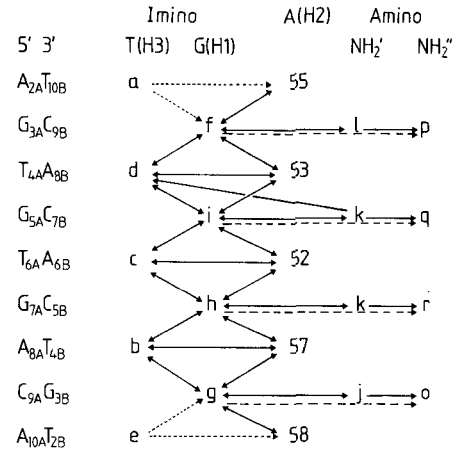

Fig. 5. *Flow chart of the NOEs observed on the duplex 11mer in 90% H_2O/10% D_2O at 23 °C involving the exchangeable proton resonances.* The continuous lines (———) represent direct NOEs, the interrupted lines (– – –) indirect NOEs, and the dashed lines (--------) NOEs that could only be observed at a temperature of 10 °C and lower

Assignment of the exchangeable proton resonances

Assignment of the exchangeable proton resonances of the duplex 11mer in 90% H_2O/10% D_2O was based on pre-steady-state NOE measurements irradiating for 0.8 s in turn all imino, A(H2) and amino proton resonances (see Fig. 2) with the exception of the amino proton resonances m – r. Irradiation of the latter was not feasible as these are located too close to the water resonance such that perturbation of the water resonance magnetization by the irradiating pulse is unavoidable. The flow chart of observed NOEs is given in Fig. 5 and the assignments in Table 4. All NOEs involving the imino and A(H2) resonances were reciprocal with the exception of those involving the imino proton resonances a and e. In the latter two case, NOEs could be observed on other resonances following irradiation of resonances a and e at 10 °C but not vice versa. This is simply due to the fact that resonances a and e are very broad so that it is very difficult to detect small changes in their intensity.

Fig. 6 illustrates a few examples of pre-steady-state NOE measurements involving the exchangeable proton resonances. Irradiation of the T_{6A}(H3) resonance c (Fig. 6A) results in an intra-base-pair NOE on the A_{6B}(H2) resonance (peak 52) and in two inter-base-pair NOEs to resonances h and i of the adjacent imino protons G_{3B}(H1) and G_{5A}(H1) respectively. These inter-base-pair NOEs are also observed on irradiation of

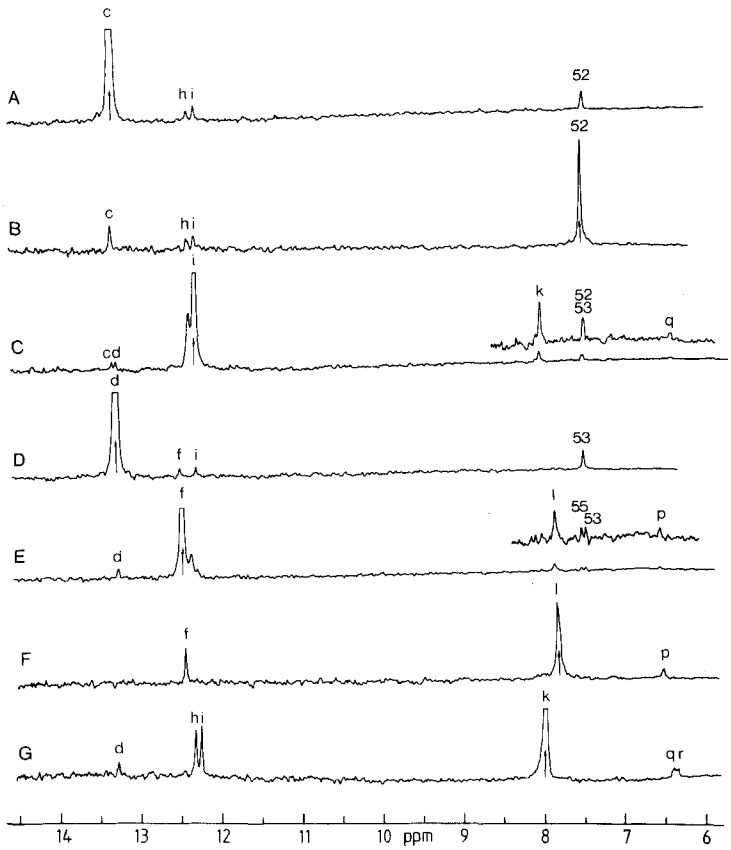

Fig. 6. *500-MHz pre-steady-state NOE difference spectra (off-resonance minus on-resonance irradiation) on the duplex 11mer in 90% H_2O/10% D_2O at 23 °C following irradiation for 0.8 s of various resonance peaks.* (A) The T_{8A}(H3) resonance c; (B) the A_{6B}(H2) resonance 52; (C) the G_{5A}(H1) resonance i; (D) the T_{4A}(H3) resonance d; (E) the G_{3A}(H1) resonance f; (F) the $C_{9B}(NH_2')$ resonance l; and (G) the $C_{7B}(NH_2')/C_{5B}(NH_2')$ resonance k. The assignments of other peaks seen in the difference spectra are given in Table 4. 1600 transients were averaged for each difference spectrum. The experimental conditions are the same as those in the Fig. 1 legend except that the sample is in 90% H_2O/10% D_2O

the A_{6B}(H2) resonance 52 (Fig. 6B). Irradiation of the G_{5A}(H1) imino proton resonance i (Fig. 6C) then results in intra-base-pair NOEs to the amino proton resonances k and q and to inter-base-pair NOEs to resonances c and d of the adjacent imino proteins T_{6A}(H3) and T_{4A}(H3), respectively, and to resonances 52 and 53 of the adjacent A_{6B}(H2) and A_{8B}(H2) protons respectively. A similar pattern of NOEs is also observed upon irradiation of the T_{4A}(H3) (peak d) and G_{3A}(H1) (peak f) imino proton resonances (see Fig. 6D and E).

Fig. 6F and G show the effects of irradiation of the amino proton resonances l and k which are associated with the $G_{3A} \cdot C_{9B}$ base pair and the $G_{5A} \cdot C_{7B}$ and $G_{7A} \cdot C_{5B}$ base pairs, respectively. In both cases we observe intra-base-pair NOEs of $\approx -15\%$ on the associated G(H1) imino proton resonances and intra-base-pair NOEs of $\gtrsim -80\%$ on high-field amino proton resonances (namely, peak p in the case of irradiation of peak l, and peaks q and r upon irradiation of peak k). (It should be noted that the intensity of the signals falls off rapidly as one approaches the water resonance owing to the nature of the excitation function the 1-1 pulse used to suppress the water resonance; see Fig. 2C. Consequently, the intra-base-pair NOEs observed on the high-field amino proton resonances p, q and r appear small in the difference spectra in Fig. 6 although in fact they are very large.) Thus peaks k and l can be assigned to hydrogen-bonded amino protons and peaks p, q and r to the corresponding non-hydrogen-bonded amino protons. These amino protons could either arise from the $C(NH_2)$ or $G(NH_2)$ protons; a distinction between these two possibilities cannot be made reliably at present. The identity of the exchangeable amino protons resonances m and n (see Fig. 2), which presumably arise from slowly exchanging $A(NH_2)$ protons, could not be ascertained from the NOE measurements.

The solution structure of the duplex 11mer

Because of the r^{-6} dependence of the pre-steady-state NOE, the relative magnitude of the NOEs provide a sensitive probe which can be used to obtain a qualitative view of the solution structure of the duplex 11mer. The pattern of intranucleotide and internucleotide NOEs observed from one residue to the next are remarkably similar, indicative of a fairly regular structure.

Considering the intranucleotide NOEs first, we observe large intranucleotide NOEs (-20% to -30%) between the H8/H6 and H2′ protons, and medium to small intranucleotide NOEs ($\lesssim -8\%$) between the H8/H6 and H1′ protons and between the H8/H6 and H3′ protons (in those cases where the H3′ resonance is not buried under the residual HOD resonance). In addition, the large intranucleotide NOEs (-20% to -30%) between the H1′ and H2″ sugar protons are always a factor of 1.5–3-times larger than those between the corresponding H1′ and H2′ protons. This pattern of intranucleotide NOEs is indicative of an *anti* conformation about the glycosidic bond with the glycosidic bond torsion angle χ lying in the range $-115° \pm 30°$ and a deoxyribose conformation in the C1′-*exo* to C2′-*endo* range [36, 37], characteristic of B DNA

[48–50]. In A DNA, where the glycosidic bond and sugar pucker conformations are low *anti* and 3′-*endo* respectively [49–52], medium to small intranucleotide NOEs would be expected between the H8/H6 and H2′ protons and large ones between the H8/H6 and H3′ protons.

The sugar pucker can also be ascertained from the $J_{1'2'}$ coupling constants using the approximate empirical relationship: percentage 2′-*endo* $\approx 10 J_{1'2'}$ [53, 54]. Because of overlap of the H1′ resonances, $J_{1'2'}$ could only be determined by simulation for 7 out of the 22 residues: namely, T_{6A} (8.0 Hz), C_{9A} (8.5 Hz), A_{10A} (8.5 Hz) and T_{11A} (7.0 Hz) for the A strand, and A_{1B} (7.5 Hz), T_{2B} (9.5 Hz) and T_{11B} (7.0 Hz) for the B strand. On the basis of this data it can be deduced that the internal residues (T_{6A}, C_{9A}, A_{10A} and T_{2B}) attain 2′-*endo* conformational purities of $\gtrsim 80\,\%$ where the external residues (A_{1B}, T_{11B}, and T_{11A}) are slightly less conformationally pure (70–75 % 2′-*endo*). This is in agreement with previous findings on other short oligonucleotides [55, 56].

Turning to the internucleotide NOEs, we note that medium-sized NOEs (−10 % to −15 %) are observed between the T(CH_3) protons and the H8/H6 protons of the adjacent 5′ residue, and medium to small NOEs (−4 % to −8 %) between the C(H5) protons and the H8/H6 protons of the adjacent 5′ residue. No internucleotide NOEs, however, are observed between either the T(CH_3) or C(H5) protons and the H8/H6 protons of the adjacent 3′ residue. This pattern of internucleotide NOEs is indicative of a right-handed helix [36, 37, 57]. In addition, the internucleotide NOEs between the H2′ and H2″ protons and the H8/H6 protons of the adjacent 3′ residue are always much smaller than the intranucleotide NOEs between the H2′ and H8/H6 protons. This confirms the overall B-type conformation, as in A DNA the H2′ proton is much closer to the H8/H6 proton of the 3′ residue than to the H8/H6 proton of its own residue [34–37].

CONCLUDING REMARKS

In the present paper we have demonstrated the power of intranucleotide and internucleotide pre-steady-state NOE measurements in obtaining complete resonance assignments of the exchangeable and non-exchangeable base protons, methyl protons and H1′, H2′ and H2″ sugar protons of a relatively long non-self-complementary double-stranded DNA oligonucleotide, namely a duplex 11mer comprising a portion of the specific target site for CRP within the *gal* operon. In addition to assignments, the relative magnitudes of the NOEs are readily interpreted in a qualitative manner to yield low-resolution structural information. In the case of the duplex 11mer, the NOE data are indicative of a B-type conformation in solution in agreement with the previous circular dichroic studies [15].

With the availability of the extensive assignments presented here, the way forward is now at hand to study the basis of the specificity of the interaction of CRP with the duplex 11mer. Particularly useful in such studies will be transferred NOE measurements [20, 22, 28, 29, 58, 59] to assess the conformation of the duplex 11mer bound to CRP and NOEs between CRP and the duplex 11mer to determine regions of protein-DNA contact.

This work was supported by the Medical Research Council (GMC and AMG) and the Lister Institute of Preventive Medicine (GMC). GMC is a Lister Institute Research Fellow. All NMR spectra were recorded on the AM500 spectrometer of the Medical Research Council Biomedical NMR Centre at the National Institute for Medical Research.

REFERENCES

1. Zubay, G., Schwartz, A. & Beckwith, J. (1970) *Proc. Natl Acad. Sci. USA 66*, 104–110.
2. Epstein, W., Rothman-Denes, L. B. & Hesse, J. (1975) *Proc. Natl Acad. Sci. USA 72*, 2300–2304.
3. de Crombrugghe, B. & Pastan, I. (1978) in *The Operon* (Miller, J. H. & Reznikoff, W. D., eds) pp. 303–323, Cold Spring Harbor Laboratory Press, New York.
4. Ebright, R. H. (1982) in *Molecular Structure and Biological Function* (Griffen, J. & Duax, W., eds) pp. 99–110, Elsevier, Amsterdam, New York.
5. de Crombrugghe, B., Chen, B., Anderson, W., Nissley, P., Gottesman, N. & Pastan, I. (1971) *Nat. New Biol. 231*, 139–142.
6. Ogden, S., Haggerty, D., Stoner, C. M., Kolodrubetz, D. & Schleif, R. (1980) *Proc. Natl Acad. Sci. USA 77*, 3346–3350.
7. Aiba, H. (1983) *Cell 32*, 141–149.
8. Movva, R. N., Green, P., Nakamura, K. & Inouye, M. (1981) *FEBS Lett. 128*, 186–190.
9. Musso, R. E., Di Lauro, R., Adhya, S. & de Crombrugghe, B. (1977) *Cell 12*, 847–854.
10. Dickson, R. C., Abelson, J. N., Barnes, W. M. & Reznikoff, W. S. (1975) *Science (Wash. DC) 182*, 27–31.
11. Gilbert, W. (1976) in *RNA Polymerase* (Losick, R. & Chamberlin, M., eds) pp. 193–205, Cold Spring Harbor Laboratory Press, New York.
12. McKay, D. B. & Steitz, T. A. (1981) *Nature (Lond.) 290*, 744–749.
13. O'Neill, M. C., Amass, K. & de Crombrugghe, B. (1981) *Proc. Natl Acad. Sci. USA 78*, 2213–2217.
14. Ebright, R. H. & Wong, J. R. (1981) *Proc. Natl Acad. Sci. USA 78*, 4011–4015.
15. Martin, S. R., Gronenborn, A. M. & Clore, G. M. (1983) *FEBS Lett. 159*, 102–106.
16. Fried, M. G. & Crothers, D. M. (1983) *Nucleic. Acids Res. 11*, 141–158.
17. Kolb, A. & Buc, H. (1982) *Nucleic. Acids Res. 10*, 473–485.
18. Unger, B., Clore, G. M., Gronenborn, A. M. & Hillen, W. (1983) *EMBO J. 2*, 289–293.
19. McKay, D. B., Weber, I. T. & Steitz, T. A. (1983) *J. Biol. Chem. 257*, 9518–9524.
20. Gronenborn, A. M. & Clore, G. M. (1982) *Biochemistry 21*, 4040–4048.
21. Clore, G. M. & Gronenborn, A. M. (1982) *Biochemistry 21*, 4048–4053.
22. Clore, G. M. & Gronenborn, A. M. (1982) *FEBS Lett. 145*, 197–202.
23. Taniguchi, T., O'Neill, M. C. & de Crombrugghe, B. (1979) *Proc. Natl Acad. Sci. USA 76*, 5090–5094.
24. Noggle, J. & Schirmer, R. E. (1971) *The Nuclear Overhauser Effect – Chemical Applications*, Academic Press, New York.
25. Redfield, A. G. & Gupta, R. K. (1971) *Cold Spring Harbor Symp. Quant. Biol. 36*, 405–419.
26. Poulsen, F. M., Hosch, J. C. & Dobson, C. M. (1980) *Biochemistry 19*, 2956–2607.
27. Wagner, G. & Wüthrich, K. (1982) *J. Mol. Biol. 155*, 347–366.
28. Gronenborn, A. M. & Clore, G. M. (1982) *J. Mol. Biol. 155*, 160–165.
29. Clore, G. M., Gronenborn, A. M., Mitchinson, C. & Green, N. G. (1982) *Eur. J. Biochem. 128*, 113–114.
30. Roy, S. & Redfield, A. G. (1983) *Biochemistry 22*, 1386–1390.
31. Hare, D. R. & Reid, B. R. (1982) *Biochemistry 21*, 5129–5135.
32. Heerschap, A., Haasnoot, C. A. G. & Hilbers, C. W. (1982) *Nucleic. Acids Res. 10*, 6981–7000.
33. Scheek, R. M., Russo, N., Boelers, R. & Kaptein, R. (1983) *J. Am. Chem. Soc. 105*, 2914–2916.
34. Reid, A. G., Salisbury, S. A., Bellard, S., Shakked, Z. & Williams, D. H. (1983) *Biochemistry 22*, 2019–2025.
35. Reid, A. G., Salisbury, S. A., Brown, T., Williams, D. H., Vasseur, J.-J., Rayner, B. & Imbach, J. L. (1983) *Eur. J. Biochem. 135*, 307–314.

36. Clore, G. M. & Gronenborn, A. M. (1983) *EMBO J. 2*, 2109–2115.
37. Gronenborn, A. M., Clore, G. M. & Kimber, B. J. (1984) *Biochem. J.*, in the press.
38. Gait, M. J., Matthes, H. W. D., Singh, M., Sproat, B. S. & Titmas, R. C. (1982) in *Chemical and Enzymatic Synthesis of Gene Fragments – a Laboratory Manual* (Gassen, H. G. & Lang, A., eds) pp. 1–42, Verlag Chemie, Weinheim.
39. Clore, G. M., Gronenborn, A. M. & Kimber, B. J. (1983) *J. Magn. Reson. 54*, 170–173.
40. Dobson, C. M., Olejniczak, E. T., Poulsen, F. M. & Ratcliffe, R. G. (1982) *J. Magn. Reson. 48*, 87–110.
41. Roth, K., Kimber, B. J. & Feeney, J. (1980) *J. Magn. Reson. 41*, 302–309.
42. Haasnoot, C. A. G. & Hilbers, C. W. (1982) *Biopolymers 22*, 1259–1266.
43. Mellema, J. R., Haasnoot, C. A. G., van Boom, J. H. & Altona, C. (1981) *Biochim. Biophys. Acta 655*, 256–264.
44. Tran-Dinh, S., Newman, J. M., Huyn-Dinh, T., Gemissel, B., Ingolen, J. & Simonds, G. (1982) *Eur. J. Biochem. 124*, 415–425.
45. Crothers, D. M., Hilbers, C. W. & Shulman, R. O. (1973) *Proc. Natl Acad. Sci. USA 70*, 2899–2901.
46. Wagner, G. & Wüthrich, K. (1979) *J. Magn. Reson. 33*, 675–680.
47. Clore, G. M., Gronenborn, A. M., Piper, E. A., McLaughlin, L. W., Graeser, E. & van Boom, J. H. (1984) *Biochem. J.*, in the press.
48. Dickerson, R. E. & Drew, H. R. (1981) *J. Mol. Biol. 149*, 761–786.
49. Arnott, S. & Hukins, D. W. L. (1972) *Biochem. Biophys. Res. Commun. 47*, 1504–1509.
50. Dickerson, R. E., Drew, H. R., Conner, B. N., Wing, R. M., Fratini, A. V. & Kopka, M. L. (1982) *Science (Wash. DC) 216*, 475–485.
51. Conner, B. N., Takano, T., Tanaka, S., Itakura, K. & Dickerson, R. E. (1982) *Nature (Lond.) 295*, 294–299.
52. Shakked, Z., Rabinovich, D., Kennard, O., Cruse, W. B. T., Salisbury, S. A. & Viswamitra, M. A. (1983) *J. Mol. Biol. 166*, 183–201.
53. Lee, C. H. & Tinoco, I. (1980) *Biophys. Chem. 11*, 283–294.
54. Cheng, D. M., Kan, L.-S., Leutzinger, E. E., Jayaraman, K., Miller, P. S. & Ts'o, P. O. P. (1982) *Biochemistry 21*, 621–630.
55. Kan, L.-S., Cheng, D. M., Jayaraman, K., Leutzinger, E. E., Miller, P. S. & Ts'o, P. O. P. (1982) *Biochemistry 21*, 6723–6732.
56. Sanderson, M. R., Mellema, J.-R., van der Marel, G. A., Wille, G., van Boom, J. H. & Altona, C. (1983) *Nucleic. Acids Res. 11*, 3333–3345.
57. Feigon, J., Wright, J. M., Leupin, W., Denny, W. A. & Kearns, D. R. (1982) *J. Am. Chem. Soc. 104*, 5540–5541.
58. Clore, G. M. & Gronenborn, A. M. (1982) *J. Magn. Reson. 48*, 402–417.
59. Clore, G. M. & Gronenborn, A. M. (1983) *J. Magn. Reson. 53*, 423–442.

G. M. Clore and A. M. Gronenborn,
Division of Physical Biochemistry, National Institute for Medical Research of the Medical Research Council,
The Ridgeway, Mill Hill, London, England NW7 1AA